Superlattices and Microstructures 49 (2011) 477–486

Contents lists available at ScienceDirect

Superlattices and Microstructures

journal homepage: www.elsevier.com/locate/superlattices

Effect of preheating temperatures on microstructure and optical properties of Na-doped ZnO thin films by sol–gel process

Jianguo Lv [a,b], Kai Huang [c], Xuemei Chen [a], Jianbo Zhu [a], Lijun Wang [a], Xueping Song [b], Zhaoqi Sun [b,*]

[a] Department of Physics and Electronic Engineering, Hefei Normal University, Hefei 230061, PR China
[b] School of Physics and Material Science, Anhui University, Hefei 230039, PR China
[c] Department of Mathematics & Physics, Anhui University of Architecture, Hefei 230601, PR China

ARTICLE INFO

Article history:
Received 8 October 2010
Received in revised form
30 December 2010
Accepted 22 January 2011
Available online 31 January 2011

Keywords:
Na-doping
Residual stress
Preheating temperature
Photoluminescence spectra

ABSTRACT

The chemical composition, crystalline structure, surface morphology and photoluminescence spectra of Na-doped ZnO thin films with different heat treatment process were investigated by X-ray photoelectron spectroscopy, X-ray diffraction, atomic force microscopy and a fluorescence spectrometer. The results show that preferred orientation, residual stress, average crystal size and surface morphology of the thin films are strongly determined by the preheating temperature. The effects of preheating temperature on microstructure and surface morphology have been discussed in detail. The photoluminescence spectra show that there are strong violet & UV emission, blue emission and green emission bands. The violet & UV emission is ascribed to the electron transition from the localized level below the conduction band to the valence band. The blue emission is attributed to the electron transition from the shallow donor level of oxygen vacancies to the valence band, and the electron transition from the shallow donor level of interstitial zinc to the valence band. The green emission is assigned to the electron transition from the level of ionized oxygen vacancies to the valence band.

* Corresponding author. Tel.: +86 551 5107284, +86 551 3674132; fax: +86 551 5107237.
E-mail addresses: szq@ahu.edu.cn, lvjg1@163.com (Z. Sun).

0749-6036/$ – see front matter © 2011 Elsevier Ltd. All rights reserved.
doi:10.1016/j.spmi.2011.01.005

1. Introduction

Zinc oxide(ZnO) is a II–VI group compound semiconductor with a wide band gap. ZnO has a hexagonal wurtzite structure ($c = 0.5207$ nm, $a = 0.3250$ nm) with oxygen atoms on hexagonal sites and zinc atoms on tetrahedral sites. ZnO is used in many applications such as solar cells [1], laser devices [2], gas sensor devices [3] and short wavelength light emitting diodes [4]. In particularly, the highly preferential orientation along the *c*-axis of ZnO thin films is a useful characteristics in optical wave-guides, surface acoustic wave and acoustic–optic devices [5,6]. Therefore, potential device applications in optoelectronics necessitate better understanding of the factors controlling the structural and optical properties of the thin films. Various dopants are known to enhance the structural and optical properties of ZnO thin films [7,8]. However, less attention has been paid to Na doping in ZnO. The doping of Na in ZnO [9,10] is expected to modify the nanostructure, surface morphology, and luminescent and other physical or chemical properties of ZnO.

ZnO thin films have been prepared by a variety of methods such as magnetron sputtering [11], pulsed laser deposition (PLD) [12], spray pyrolysis [13], chemical vapor deposition (CVD) [14], molecular beam epitaxy (MBE) [15] and sol–gel processing [16,17]. The sol–gel process is one of the versatile methods to prepare thin film without complicated instruments. It is simple, inexpensive, and has a general advantage of large area deposition and uniformity of the films' thickness. For the ZnO thin films prepared by the sol–gel method, the structural and optical properties can be controlled by preheating temperature and annealing temperature [18–20]. Many studies to control preferential orientation and optical properties have concentrated on the annealing treatment. However, the effects of preheating temperature have rarely been studied [20,21].

In this study, the experimental results of crystalline structure, residual stress, surface morphology and photoluminescence (PL) of Na-doped ZnO thin films with different heat treatment process have been investigated, with aim of improving the structural and optical properties of Na-doped ZnO films.

2. Experimental

Zinc acetate dehydrate ($Zn(COOCH_3)_2 \cdot 2H_2O$) and sodium chloride (NaCl) were used as the starting salt materials to prepare Na-doped ZnO thin films by the sol–gel method. The flow chart of the preparation of Na-doped ZnO thin films is shown in Fig. 1.

The zinc acetate dihydrate and sodium chloride were dissolved in ethylene glycol monomethyl ether ($HOCH_2CH_2OCH_3$) and monoethanolamine (MEA) solution at room temperature. The atomic ratio of Na/Zn was 0.08. The concentration of zinc acetate was 0.5 mol/L and the molar ratio of MEA to ZnAc was kept to 1.0. The choice of 0.08 for the Na/Zn atomic ratio and 0.5 mol/l as the concentration of zinc acetate was justified from our previous researches. The mixture was stirred by a magnetic stirrer at 60 °C until a clear and homogeneous solution formed. The sol–gel coating was made usually 1day after the solution was prepared. Silicon was used as the supporting substrate. The thin films were obtained by a spin-coating method at 3000 rpm for 30 s. The thin films were preheated at temperatures ranging from 150 to 250 °C for 10 min. The coating and the preheating treatment processes were repeated ten times to get about 300 nm thick Na-doped ZnO thin films. The thin films were then annealed at temperatures ranging from 400 to 800 °C in air for 60 min. Table 1 lists the sample numbers and the preheating and annealing temperatures.

The thermal decomposition behavior of the Na-doped ZnO precursor sol solution was examined by a thermogravimetry analyzer (TGA, NETZSCH STA 449F3). Composition of the Na-doped ZnO thin film was investigated by X-ray photoelectron spectroscopy (XPS, Thermo-VG Scientific ESCALAB250). The crystal structure of the thin films was examined by X-ray diffraction (XRD, MACM18XHF) employing CuKα radiation. The preferred growth of the (*hkl*) planes has been expressed in terms of a texture coefficient $T_{c(hkl)}$. Quantitative information concerning the degree of preferential orientation can been obtained from the texture coefficient, T_c, defined as [22,23]:

$$T_{c(hkl)} = \frac{(I_{(hkl)}/I_{r(hkl)})}{\left[\left(\sum I_{(hkl)}/I_{r(hkl)}\right)/n\right]} \quad (1)$$

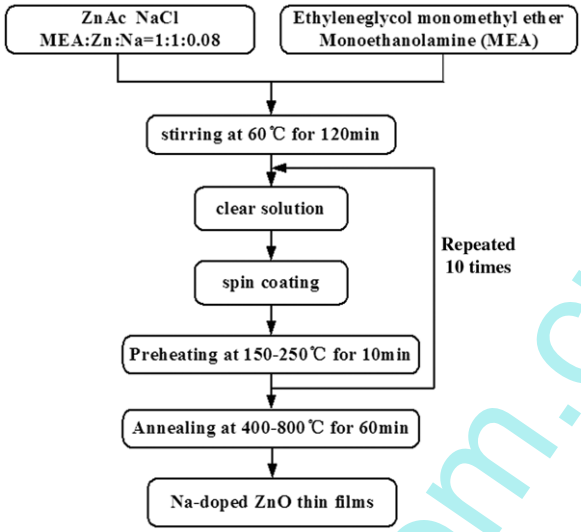

Fig. 1. Flow chart of sol–gel method for preparation of Na-doped ZnO thin films.

where $I_{(hkl)}$ are the XRD intensities of the thin films, n is the number of diffraction peaks considered, and $I_{r(hkl)}$ are the intensities of the XRD reference (JCPDS card 36-1451) of the randomly oriented crystallites. A sample with randomly oriented crystallites presents a $T_{c(hkl)}$ of 1, while a larger value indicates an abundance of crystallites oriented to the (*hkl*) plane. The surface morphology of the thin films was characterized by an atomic force microscope (AFM, CSPM-4000) operating in contact mode. The photoluminescence (PL) spectra of the thin films were measured in the wavelength region of 350–600 nm at room temperature by a fluorescence spectrometer (FL, F-4500FL) with a xenon lamp as light source excited at 325 nm. A cutoff filter to pass only long waves above 350 nm was used to block the lights scattered from the source.

3. Results and discussion

3.1. Thermal analysis of Na-doped ZnO sol solution

Fig. 2 shows TGA curve of a Na-doped ZnO sol solution. Weight losses were observed in three temperature regions 60 °C–120 °C, 130 °C–230 °C and 240 °C–270 °C. The first weight loss is due to the evaporation of ethylene glycol monomethyl ether and water. Second and third weight losses are caused by the evaporation of water and the decomposition of residual organics and MEA, respectively.

3.2. XPS analysis

A typical XPS survey spectrum of the thin films preheated at 150 °C and annealed at 800 °C is shown in Fig. 3(a). The elements of C, O, Zn and Na were detected in the spectrum. The presence of a C1s peak in spectrum can be attributed to contamination which resulted from residual organic solvents and the samples being exposed to ambient atmosphere. A high resolution scan for C, O, Zn and Na was performed. The XPS peak of Na1s of the sample is shown in Fig. 3(b). According to the high resolution scan spectrum, the atomic concentrations of elements are computed from the measured peak area together with the sensitivity factors [24]. The obtained atomic concentrations of C, O, Zn and Na are 20.9, 40.9, 36.9 and 1.3 at.%, respectively. The corresponding XPS results of the thin film are summarized in Table 2. The results show that the value of the Na/Zn ratio in the thin film surface (0.034) is much smaller than that in solution (0.080).

Table 1
Microstructure, residual stress and RMS roughness of the samples.

Sample no.	Preheating temperature (°C)	Annealing temperature (°C)	$T_{c(100)}$	$T_{c(002)}$	$T_{c(101)}$	$T_{c(103)}$	Average crystal size (nm)	Lattice constants (nm)		Residual stress (%)	RMS roughness (nm)
								a	*c*		
1#	150	400	0.873	2.135	0.588	0.402	16.9	0.3258	0.5217	0.195	8.0
2#	200	400	1.521	1.185	0.960	0.332	16.7	0.3250	0.5199	−0.154	7.1
3#	250	400	–	–	–	–	4.6	–	–	–	3.9
4#	150	600	0.582	2.408	0.453	0.557	28.4	0.3251	0.5209	0.045	16.4
5#	200	600	1.116	1.625	0.908	0.349	21.8	0.3249	0.5204	−0.064	11.0
6#	250	600	0.758	3.242	–	–	21.4	0.3237	0.5187	−0.392	7.9
7#	150	800	0.376	2.389	0.340	0.895	31.5	0.3256	0.5215	0.149	23.4
8#	200	800	1.566	1.406	1.028	–	30.3	0.3240	0.5198	−0.174	17.4
9#	250	800	0.968	2.267	0.764	–	30.1	0.3235	0.5191	−0.300	8.3

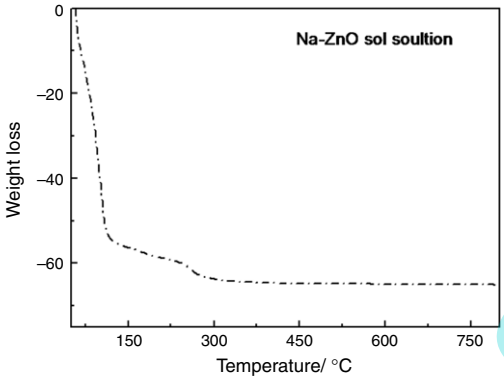

Fig. 2. TGA curve of Na-doped ZnO sol solution.

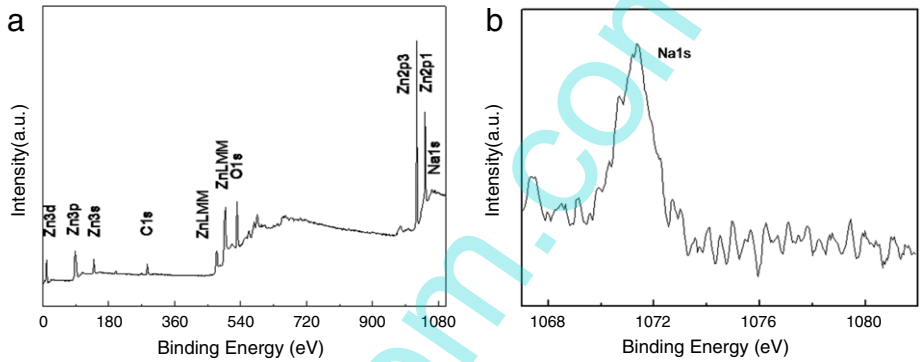

Fig. 3. XPS survey spectrum (a) and high resolution scan spectrum of Na1s (b) for the sample preheated at 150 °C and annealed at 800 °C.

Table 2
The XPS results of the thin film preheated at 150 °C and annealed at 800 °C.

Element	Area	Sensitivity factor	Atomic concentration (%)
C1s	21 065	0.25	20.9
O1s	96 411	0.66	40.9
Zn2p3	405 262	4.80	36.9
Na1s	6 136	2.30	1.3

3.3. Structure and orientation of Na-doped ZnO thin films

Fig. 4 shows the XRD patterns of Na-doped ZnO thin films prepared by preheated at 150, 200, and 250 °C and annealed at 400 °C, 600 °C, and 800 °C, respectively. These patterns correspond to diffraction peaks of polycrystalline ZnO at (100), (002), (101), (102), (110), (103) and (112) planes (JCPDS card 36-1451). The results reveal that all the thin films have a hexagonal wurzite structure. The texture coefficients, $T_{c(100)}$, $T_{c(002)}$, $T_{c(101)}$, and $T_{c(103)}$, of the thin films are calculated and shown in Table 1. It is seen that the texture coefficient varies with preheating temperatures. From Fig. 4 and Table 1, it can be seen that the thin films prepared with preheating at 200 °C do not exhibit a preferred orientation. Other thin films deposited with preheating at 150 °C and 250 °C exhibit a preferred *c*-axis orientation. The mechanism of formation of the *c*-axis preferentially oriented ZnO thin film can suggest that the value of the surface free energy is a minimum for the ZnO(002) plane at the growth stage [25].

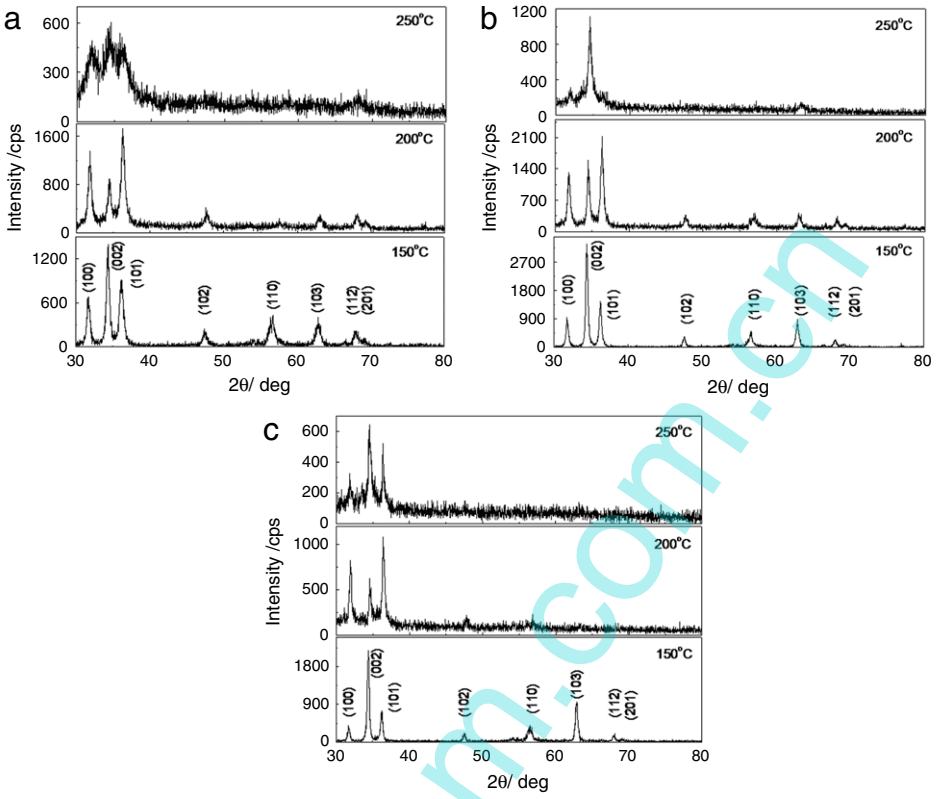

Fig. 4. XRD patterns of Na-doped ZnO thin films with different preheating and annealing temperatures, (a) preheated at 150, 200 and 250 °C and annealed at 400 °C, (b) preheated at 150, 200 and 250 °C and annealed at 600 °C, and (c) preheated at 150, 200 and 250 °C and annealed at 800 °C.

3.4. Lattice constants and crystal sizes of the thin films

The lattice parameters can be calculated by using the following formula [25]:

$$d_{hkl} = \frac{1}{\sqrt{4(h^2 + k^2 + hk)/3a^2 + l^2/c^2}} \tag{2}$$

where a, c are the lattice parameters and d_{hkl} is the interplanar distance for the (hkl) planes. The lattice parameters a, c have been calculated and are summarized in Table 1.

The strain along the c-axis, ε_{zz} is given by the following equation [26]:

$$\varepsilon_{zz} = (c - c_0)/c_0 \times 100\% \tag{3}$$

where c is the lattice parameter of the strained ZnO thin films calculated from X-ray diffraction data and c_0 (0.5207) is the unstrained lattice parameter of ZnO [27]. According to the above formula, the positive value of ε_{zz} represents the tensile residual stress while a negative value represents compressive residual stress. ε_{zz} values are computed using the above relationship and are summarized in Table 1. It is seen that the annealing temperature only slightly influences the stress of the Na-doped ZnO thin films preheated at the same temperature. However, it is found that the tensile residual stress converts to compressive residual stress in the thin films annealed under the same temperature with preheating temperatures increasing from 150 to 250 °C. In general, the total stress consists of two components, thermal stress and lattice stress. The cause of the former is thermal mismatch between thin film and substrate and the generation mechanism of the latter component reflects the film's

structure. In our study, the residual stress forms mainly due to lattice mismatch stress. Bao et al. have reported that the tensile residual stresses of ZnO thin films, prepared on quartz glass by the sol–gel method, decreases with increasing preheating temperature [28]. Wang et al. have reported that the preheating temperature only slightly influences the residual stress of the ZnO thin film prepared on $Si/SiO_2/Ti/Pt$ using the sol–gel method, and the compressive residual stresses convert to tensile residual stresses in the ZnO films preheated at 400 °C with the annealing temperature increasing from 550 to 1000 °C [17]. They explained that the conversion of residual stress for the thin films could be attributed to the interaction between the thermal stress and the lattice stress.

Crystal sizes of the thin films were calculated using the Scherrer formula as follows [29]:

$$D = \frac{0.9\lambda}{\beta \cos\theta} \tag{4}$$

where $\lambda = 0.15406$ nm is the wavelength of the X-ray radiation used, θ is the Bragg diffraction angle of the XRD peak and β is the full width at half maximum (FWHM). The calculated values of the average crystal size are depicted in Table 1. It can be seen that the average crystal size for the thin films annealed under the same temperature decreases with increasing the preheating temperature.

3.5. Surface morphology of the thin films

The morphology of Na-doped ZnO thin films were investigated by AFM. Fig. 5 only shows AFM images of the thin films prepared by preheating at 150 °C–250 °C for 10 min and annealed at 800 °C for 1 h. RMS roughness of all the thin films is listed in Table 1. It can be seen that the sample preheated at 150 °C and annealed at 800 °C has some big punctures, the biggest particle sizes and the roughest surface. It also can be seen that the surface roughness of the samples annealed at the same temperature increases with an increase of preheating temperature. The reasons could be explained that the high preheating temperature benefits the decomposition of the zinc copolymers in precursor films and leaves some small pores in the films. These pores will be filled by new precursor solution in the next coating process, which makes the thin films smoother and denser. When the precursor films are preheated at lower temperature, the copolymers cannot decompose completely during the preheating treatment. The copolymers will combust during the annealing process, so big punctures and rougher surfaces are formed in the thin films [21].

3.6. Optical properties

The photoluminescence (PL) property of the ZnO thin film is one of the most interesting and important properties that has been intensively investigated recently. Fig. 6(a) shows the PL spectra obtained at room temperature for Na-doped ZnO thin films preheated at 150, 200 and 250 °C and annealed at 400 °C, respectively. The results indicated that two samples preheated at 200 and 250 °C exhibit violet and UV emission and a blue emission band in the 440–480 nm region, and no green emission band was detected. However, the sample preheated at 150 °C shows three emissions of strong violet emission, blue emission and green emission bands. The blue-shift of violet and UV emission with an increase of preheating temperature can be observed. Fig. 6(b) is the PL spectra obtained at room temperature for Na-doped ZnO thin films preheated at 150, 200 and 250 °C and annealed at 600 °C, respectively. The spectra exhibit violet and UV emission bands, weak blue emission and green emission bands. Specially, the violet and UV emission of the thin film preheated at 200 °C consists of a UV emission peak at 385 nm and violet emission peak at 415 nm. Fig. 6(c) shows the PL spectra obtained at room temperature for Na-doped ZnO thin films preheated at 150, 200 and 250 °C and annealed at 800 °C, respectively. It also can be seen that all the PL spectra show three emissions of strong violet emission, weak blue emission and green emission bands. The blue-shift of violet and UV emission with an increase of preheating temperature can also be observed. Though there is no consensus on the origin of visible emissions in ZnO films, these are mainly due to structural defects, such as zinc vacancy, oxygen vacancy, interstitial zinc and interstitial oxygen [30]. It can be concluded that the blue emission for the Na-doped ZnO thin films is attributed to the electron transition from

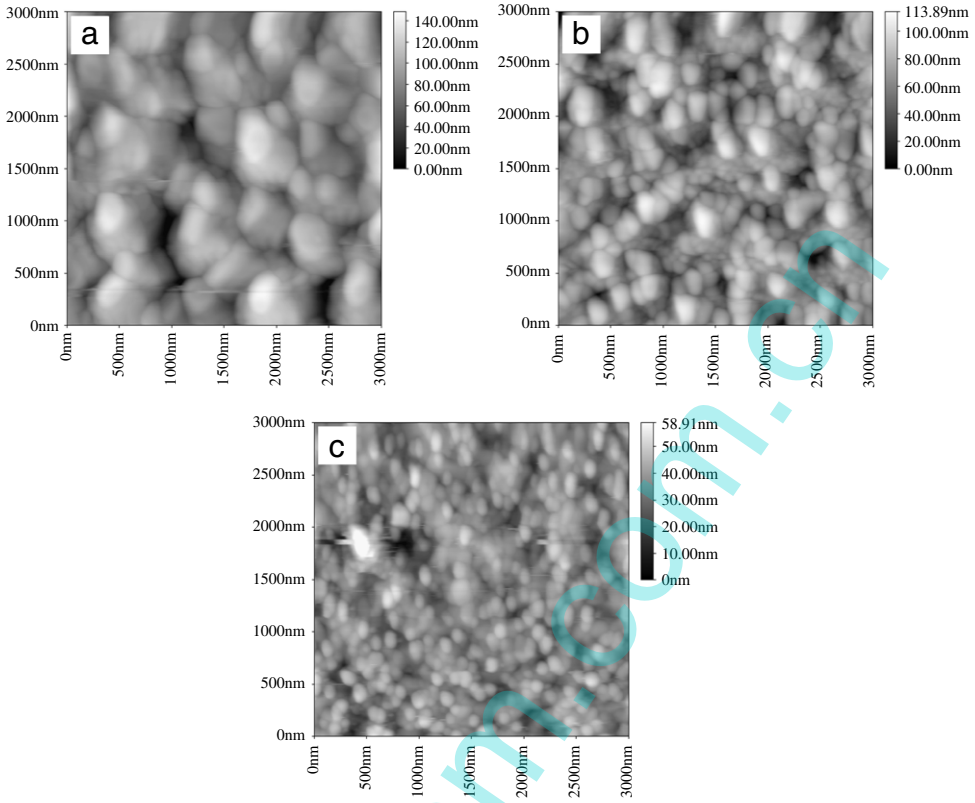

Fig. 5. AFM images of the samples preheated at 150 °C (a), 200 °C (b), 250 °C (c) and annealed at 800 °C.

the shallow donor level of oxygen vacancies to the valence band, and the electron transition from the shallow donor level of interstitial zinc to the valence band. The green emission of the thin films may be attributed to the electron transition from the level of the ionized oxygen vacancies to the valence band [31,32]. It is generally accepted that the shifts of violet and UV emission peaks of ZnO film are attributed to a change of the localized level below the conduction band [33], which originates from the free impurity atoms, the defect density of surface and interface, *c*-axis preferential orientation, and the carrier concentration above the valence band in the band gap [34,35], which may be connected with the crystal quality, *c*-axis preferred orientation and Na-incorporation.

4. Conclusion

Na-doped ZnO thin films were deposited on a silicon substrate by the sol–gel spin-coating method and the crystalline structure, residual stress, surface morphology and optical properties of the thin films with preheating temperature and annealing temperature were investigated. A Na-doped ZnO thin film with a high preferred *c*-axis orientation, smooth, homogeneous and dense surface has been prepared on a silicon substrate by using sol–gel with a preheating temperature 250 °C for 10 min and annealing temperature 600 °C for 60 min. Photoluminescence spectra of the thin films exhibit violet and UV emission, blue emission and green emission bands. The physical mechanisms of photoluminescence emissions for the thin films have been discussed in detail. The violet and UV emission and blue emission of Na-doped ZnO thin films at room temperature show a possibility of application to inorganic photoluminescence devices.

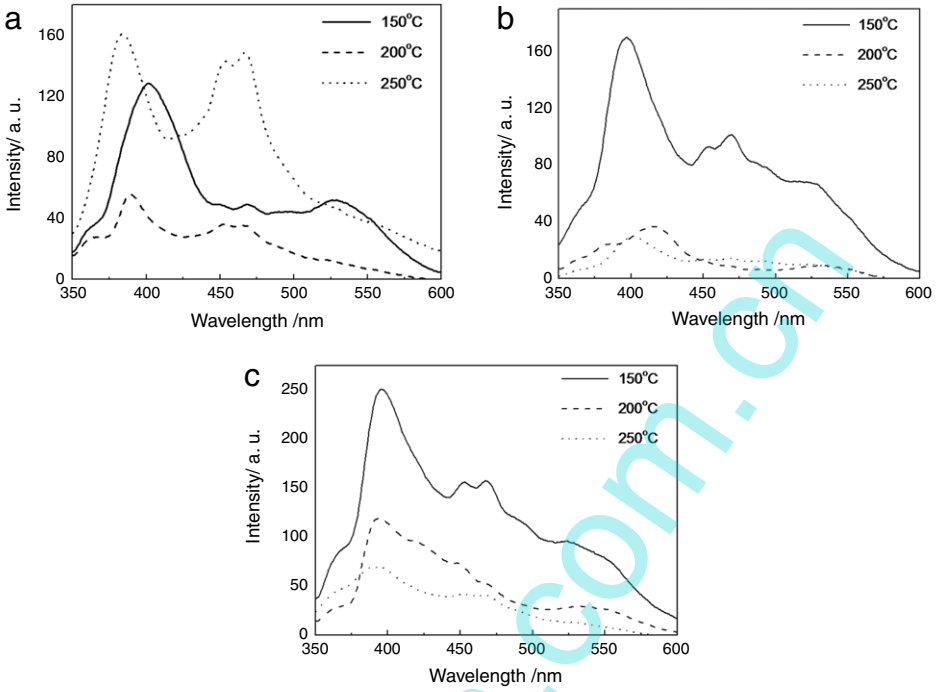

Fig. 6. PL spectra of the thin films with different preheating and annealing temperatures, (a) preheated at 150, 200 and 250 °C and annealed at 400 °C, (b) preheated at 150, 200 and 250 °C and annealed at 600 °C, and (c) preheated at 150, 200 and 250 °C and annealed at 800 °C.

Acknowledgements

This work was supported by National Natural Science Foundation of China (No. 50872001, 51072001), Research Fund for the Doctoral Program of Higher Education of China (No. 20060357003) and Natural Science Foundation of Anhui Higher Education Institution of China (No. KJ2010A284).

References

[1] J. Lee, D. Lee, D. Lim, K. Yang, Thin Solid Films 515 (2007) 6094–6098.
[2] S.S. Lee, R.P. Ried, R.M. White, Journal of Microelectromechanical Systems 5 (1996) 238–242.
[3] D.L. DeVoe, Sensors Actuators A 88 (2001) 263–272.
[4] A. Tsukazaki, A. Ohtomo, T. Onuma, M. Ohtani, T. Makino, M. Sumiya, K. Ohtani, S.F. Chichibu, S. Fuke, Y. Segawa, H. Ohno, H. Koinuma, M. Kawasaki, Nature Materials 4 (2005) 42–46.
[5] H. Sato, T. Minami, Y. Tamura, S. Sakata, T. Mori, N. Ogawa, Thin Solid Films 246 (1994) 86–91.
[6] Z.B. Bahsi, A.Y. Oral, Optical Materials 29 (2007) 672–678.
[7] H.X. Chen, J.J. Ding, S.Y. Ma, Physica E 42 (2010) 1487–1491.
[8] S.J. Henley, M.N.R. Ashfold, D. Cherns, Surface and Coatings Technology 177–178 (2004) 271–276.
[9] D.Y. Wang, S.X. Gao, Journal of Alloys and Compounds 476 (2009) 925–928.
[10] B. Karthikeyan, C.S. Suchand Sandeep, T. Pandiyarajan, P. Venkatesan, R. Philip, Applied Physics Letters 95 (2009) 023118.
[11] K.H. Lee, N.I. Cho, E.J. Yun, H.G. Nam, Applied Surface Science 256 (2010) 4241–4245.
[12] X.Q. Wei, Z. Zhang, Y.X. Yu, B.Y. Man, Optics and Laser Technology 41 (2009) 530–534.
[13] T.P. Rao, M.C. Santhoshkumar, Applied Surface Science 255 (2009) 7212–7215.
[14] M. Purica, E. Budianu, E. Rusu, M. Danila, R. Gavrila, Thin Solid Films 403–404 (2002) 485–488.
[15] S.P. Wang, C.X. Shan, B. Yao, B.H. Li, J.Y. Zhang, D.X. Zhao, D.Z. Shen, X.W. Fan, Applied Surface Science 255 (2009) 4913–4915.
[16] C.Y. Tsay, H.C. Cheng, Y.T. Tung, W.H. Tuan, C.K. Lin, Thin Solid Films 517 (2008) 1032–1036.
[17] Y.M. Li, L.H. Xu, X.Y. Li, X.Q. Shen, A.L. Wang, Applied Surface Science 256 (2010) 4543–4547.
[18] Z.B. Fang, Z.J. Yan, Y.S. Tan, X.Q. Liu, Y.Y. Wang, Applied Surface Science 241 (2005) 303–308.
[19] L.P. Peng, L. Fang, X.F. Yang, Y.J. Li, Q.L. Huang, F. Wu, C.Y. Kong, Journal of Alloys and Compounds 484 (2009) 575–579.
[20] Y.S. Kim, W.P. Tai, S.J. Shu, Thin Solid Films 491 (2005) 153–160.

[21] M. Wang, J. Wang, W. Chen, Y. Cui, L. Wang, Materials Chemistry and Physics 97 (2006) 219–225.
[22] S. Lemlikchi, S.A. Messaci, S. Lafane, T. Kerdja, A. Guittoum, M. Saad, Applied Surface Science 256 (2010) 5650–5655.
[23] R. Romero, D. Leinen, E.A. Dalchiele, J.R. Ramos-Barrado, F. Martín, Thin Solid Films 515 (2006) 1942–1949.
[24] X.Q. Wei, B.Y. Man, M. Liu, C.S. Xue, H.Z. Zhuang, C. Yang, Physica B 388 (2007) 145–152.
[25] D. Raoufi, T. Raoufi, Applied Surface Science 255 (2009) 5812–5817.
[26] H.C. Ong, A.X.E. Zhu, G.T. Du, Applied Physics Letters 80 (2002) 941–943.
[27] R. Ghosh, D. Basak, S. Fujihara, Journal of Applied Physics 96 (2004) 2689–2692.
[28] D. Bao, H. Gu, A. Kuang, Thin Solid Films 312 (1998) 37–39.
[29] J.G. Chen, C.X. Guo, L.L. Zhang, J.T. Hu, Chinese Physics Letters 21 (2004) 1366–1369.
[30] Y.G. Wang, S.P. Lau, H.W. Lee, S.F. Yu, B.K. Tay, X.H. Zhang, H.H. Hng, Journal of Applied Physics 94 (2003) 354–358.
[31] K. Vanheusden, W.L. Warren, C.H. Seager, D.R. Tallant, J.A. Voigt, Journal of Applied Physics 79 (1996) 7983–7990.
[32] D.H. Zhang, Q.P. Wang, Z.Y. Xue, Photoluminescence of ZnO films excited with light of different wavelength, Applied Surface Science 207 (2003) 20–25.
[33] B.J. Jin, S. Im, S.Y. Lee, Thin Solid Films 366 (2000) 107–110.
[34] D. Behera, B.S. Acharya, Journal of Luminescence 128 (2008) 1577–1586.
[35] S. Cho, J. Ma, Y. Kim, Y. Sun, G.K.L. Wong, J.B. Ketterson, Applied Physics Letters 75 (1999) 2761–2763.